AIP | Applied Physics Letters

Fabrication of doubly resonant plasmonic nanopatch arrays on graphene

M. Grande, T. Stomeo, G. V. Bianco, M. A. Vincenti, D. de Ceglia et al.

Citation: Appl. Phys. Lett. **102**, 231111 (2013); doi: 10.1063/1.4810785
View online: http://dx.doi.org/10.1063/1.4810785
View Table of Contents: http://apl.aip.org/resource/1/APPLAB/v102/i23
Published by the American Institute of Physics.

Fabrication of doubly resonant plasmonic nanopatch arrays on graphene

M. Grande,[1] T. Stomeo,[2] G. V. Bianco,[3] M. A. Vincenti,[4] D. de Ceglia,[4] V. Petruzzelli,[1] G. Bruno,[3] M. De Vittorio,[2,5] M. Scalora,[6] and A. D'Orazio[1]
[1]*Dipartimento di Ingegneria Elettrica e dell'Informazione, Politecnico di Bari, Via Re David 200, 70125 Bari, Italy*
[2]*Center for Bio-Molecular Nanotechnology, Istituto Italiano di Tecnologia (IIT), Via Barsanti, Arnesano 73010, Lecce, Italy*
[3]*Institute of Inorganic Methodologies and of Plasmas, IMIP-CNR, via Orabona 4, 70126 Bari, Italy*
[4]*National Research Council – AMRDEC, Charles M. Bowden Research Laboratory, Redstone Arsenal, Alabama 35898, USA*
[5]*National Nanotechnology Laboratory (NNL), CNR-ISTITUTO DI NANOSCIENZE, Dip. Ingegneria dell'Innovazione, Università Del Salento, Via Arnesano, 73100 Lecce, Italy*
[6]*Charles M. Bowden Research Laboratory, AMRDEC, US Army RDECOM, Redstone Arsenal, Alabama 35898, USA*

(Received 8 February 2013; accepted 28 May 2013; published online 10 June 2013)

We report theoretical and experimental investigations of the optical response of two-dimensional periodic arrays of rectangular gold nanopatches grown on a monolayer graphene placed on a glass substrate. We discuss the numerical analysis and optical characterization by means of reflection spectra and show that rectangular nanopatches display a polarization-dependent response, at normal incidence, which leads to double plasmonic resonances due to the Wood anomaly. We detail the fabrication process highlighting how the resist primer and the adhesion layer can reduce and impede the graphene doping due to the environment and to the nanopatches, respectively, by means of Raman spectroscopy. © *2013 AIP Publishing LLC*. [http://dx.doi.org/10.1063/1.4810785]

Graphene is a perfect two-dimensional (2D) carbon sheet in honeycomb lattice with unique, multi-faceted properties,[1] and it is a basic building block of well-known carbon materials such as graphite, carbon nanotubes, and fullerenes. Graphene is a promising material due to its peculiar electronic properties, such as charge carriers that mimic massless Dirac fermions, electron-hole symmetry near the charge neutrality point, and weak spin-orbit coupling. Another surprising feature is related to its high mobility, its stability at ambient conditions, and scalability down to one atomic layer. At the same time, graphene has been recognized as a valid candidate for replacing transparent conductors like indium tin oxide (ITO) in solar cells since it combines low absorption (~2.3% for a monolayer) and high conductivity. This material is also highly sensitive to environmental parameters, and it can be functionalized in order to select desirable or specific species or analytes. Finally, its nonlinear response based on Raman spectroscopy may also be exploited to realize graphene-based devices with high sensitivity and selectivity.[2]

Graphene is believed to be one of the most promising candidates also in photonics and optoelectronics (graphene photonics). Very recently plasmons have been identified in graphene thus opening a research field called graphene plasmonics.[3] In this particular case, the electric field of an incident light beam can drive a collective excitation of free charges (conduction electrons) back and forth between the opposite ends of a graphene sheet, leading to the enhancement of the optical field. Moreover, graphene plasmonics provides a suitable alternative to noble-metal plasmonics, since the associated surface plasmons (SPs) exhibit much larger light confinement abilities (between one and three orders of magnitude smaller than the wavelength of light[4]) and relatively long propagation distances, with the advantage of being highly tunable via electrostatic gating. Tunability and gating are related to the possibility to vary the Fermi energy level in doped graphene sheets by applying an external electrostatic field.[5] To date, some examples of the combination of graphene and plasmonics have been reported for different applications in a number of research fields including periodic structures,[6] metamaterials,[7] Raman spectroscopy,[8,9] photodetectors,[10] THz devices,[11] photovoltaics,[12] and chemical sensing.[13]

In this paper we study the optical response of two-dimensional periodic arrays of rectangular gold nanopatches grown on a monolayer graphene placed on a glass substrate. By analyzing the optical response we show that the rectangular shape of a periodic array leads to a doubly resonant plasmonic system. We then examine the interaction between these plasmonic resonances and the graphene layer by emphasizing the variation of the optical properties in terms of absorption and resonance shift. Finally, we focus on the optimization of the fabrication technology by taking advantage of the sensitivity of Raman spectroscopy on graphene structural quality and doping. Specifically, the role of the resist primer and adhesion layer on preserving charge transport properties of graphene is investigated.

Fig. 1 shows a sketch of the rectangular array having two different periodicities along the x-axis and y-axis, labelled p_x and p_y, respectively. The inset in Fig. 1 shows the cross section of a single nanopatch on the chrome adhesion layer and graphene. The gold nanopatches are fabricated on a commercial monolayer graphene supplied by Graphene Supermarket, which is grown via Chemical Vapour Deposition (CVD) technique and transferred onto a glass substrate.

The rectangular form factor of the nanopatches ($p_x \neq p_y$) adds another degree of freedom with respect to a square geometry. These 3D square structures support three different

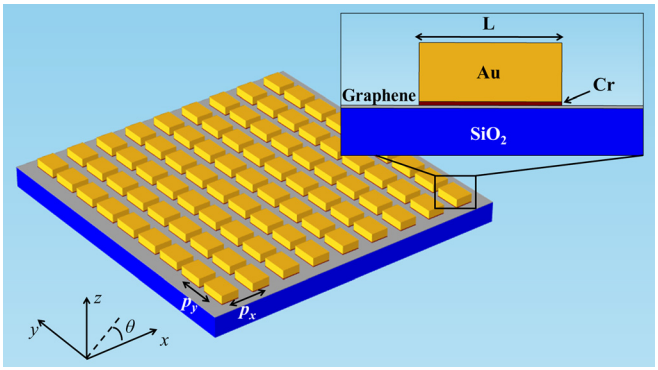

FIG. 1. (a) Sketch of the 2D array where p_x and p_y define the periodicity along the x-axis and y-axis, respectively. The polarization angle θ is defined in the xy-plane; (inset) cross-section of a single nanopatch. The aperture $a_x = a_y$ is defined as the difference between the periodicity p_x or p_y and the nanopatch length L.

resonances when illuminated by a transverse magnetic (TM) polarized field, as previously reported:[14] (i) a narrow band resonant state involving the whole grating (state V) due to the Wood anomaly as reported in Ref. 14; (ii) a leaky mode due to the coupling between a SPP (Surface Plasmon Polariton) and the impinging light (state M); and (iii) a broadband Fabry-Pérot-like resonance of the transverse-electro-magnetic (TEM) guided mode supported by the slit, which acts as a metal-insulator-metal (MIM) waveguide (state H). Additionally, square nanopatches result to be insensitive to the incident polarization as previously demonstrated in Ref. 16. In contrast, rectangular nanopatches show different behaviour with respect to incident polarization.[17] We stress that this behaviour is slightly different from the devices reported in references,[18,19] since they offer a double plasmonic resonance for the same polarization. Finally, it is worth highlighting that periodic arrangement of single dots and double-dots show similar behaviour as reported in Ref. 15. However, the rectangular nanopatches display Wood anomalies for normal incidence, and they have been designed in order to let interfere the SP mode with the Fabry-Pérot-like resonance due to the MIM waveguide. Therefore, in order to verify the sensitivity of gold rectangular nanopatches to polarization, we designed an array with main spectral features near $\lambda \sim 633$ nm and $\lambda \sim 780$ nm. In order to set these working wavelengths we performed the analysis by considering an array with periodicity $p_x = 630$ nm and $p_y = 780$ nm. The metal thickness is $w = 150$ nm.

We first analyzed the linear response by means of a simulation code based on the Finite Element Method.[20] The simulation domain contained a unit cell with a single nanopatch on a graphene layer placed on the glass substrate (as shown in the inset of Fig. 1). Although not critical in the evaluation of the reflection spectrum, the 3 nm-thick chrome adhesion layer placed between the graphene layer and the gold nanopatch has also been taken into account the calculation. Periodic boundary conditions (PBCs) were introduced to simulate the infinite array along the periodicity directions. The monolayer graphene was modelled by including an electric current sheet, $J_{x,y} = \sigma_g E_{x,y} d$, on the boundary condition for the tangential component of the magnetic field. $E_{x,y}$ are the tangential electric field components along the x and y directions while the graphene conductivity value σ_g is derived from the complex refractive index reported in Refs. 21 and 22. The thickness of a single layer of graphene is assumed equal to $d = 0.34$ nm. However, it is worth noting that the effective optical thickness of the graphene layer can vary with respect to the interlayer distance of graphite as experimentally measured in Ref. 21. Experimental data for gold and chrome have been taken from Ref. 23, while the refractive index of the glass substrate is $n_s = 1.5$. We note that the 3D simulations resemble their 2D counterparts when the polarization is along the array axes, i.e., x-axis and y-axis.[17]

Figs. 2(a) and 2(c) show the reflectance maps when the aperture size a is varied from 20 nm to 400 nm evaluated in the spectral range 600 nm–900 nm for $p_x = 630$ nm and

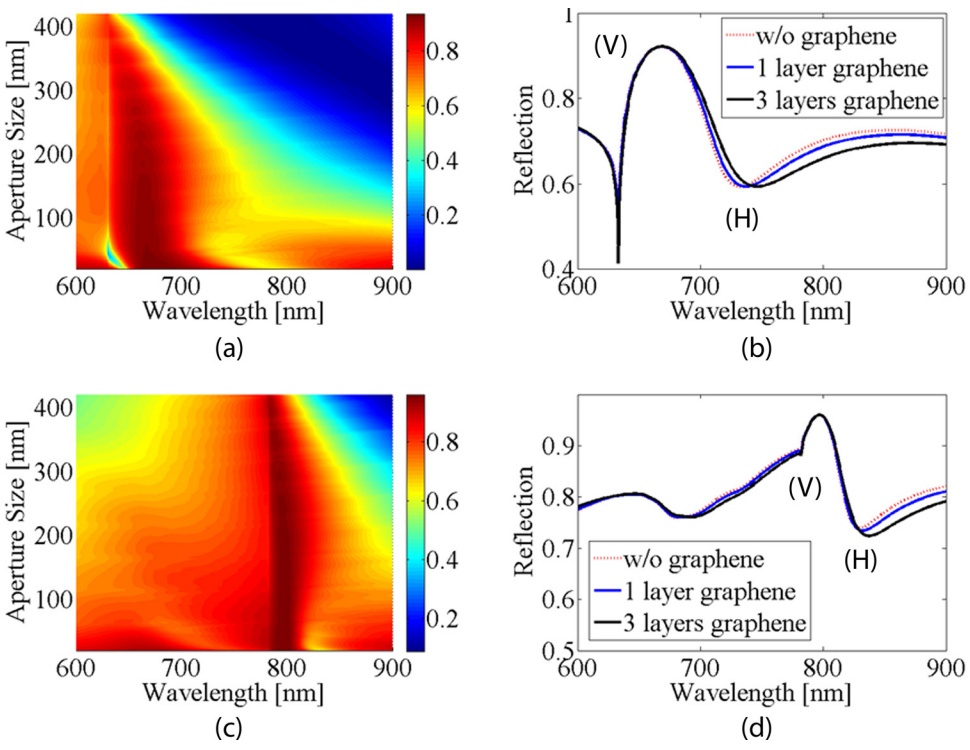

FIG. 2. Reflection maps when the polarization angle is equal to (a) 0° (electric field oriented along $p_x = 630$ nm) and (c) 90° (electric field oriented along $p_y = 780$ nm) versus the aperture size a. Reflection spectra when $a = 60$ nm (cross-section at the white dashed line) for the polarization angle equal to (b) 0° and (d) 90°, respectively, without (red dashed line) graphene, and when a single (blue line) and three (black line) graphene layers are considered.

$p_y = 780$ nm, respectively. As it can be inferred from the plots, the plasmonic resonances are located at about 633 nm and 782 nm, respectively. In order to show the effects of the graphene on the reflection spectrum of the array we plot two sections of Figs. 2(a) and 2(c) for $a = 60$ nm (see Figs. 2(b) and 2(d), respectively). In the same plots, we compare the results with a periodic array grown on a trilayer graphene and without graphene. Figs. 2(b) and 2(d) emphasize how the amount of absorption and the shift caused by the introduction of the graphene depends on to the number of layers considered in the simulations: for example, when the reflection spectrum of a structure without graphene is compared with that of a trilayer graphene and the electric field is oriented along x ($\theta = 0$, normal incidence in the plane x-z), the resonances associated to the V and H modes shift from ~633 nm (V) and ~732 nm (H) to ~634 nm (V) and 746 nm (H), respectively, when three graphene layers are considered. On the other hand, when the polarization angle is $\theta = 90°$ (y-z plane of incidence and incident electric field oriented along the y-axis), the states V and H shift from ~782 nm and ~830 nm to ~782.5 nm and ~837 nm, respectively. At the same time, the graphene layer modifies optical absorption by about few percent for both states. This behaviour may be related to the modification of the boundary conditions at the metal/air interface: the mere presence of graphene may in fact increase absorption when the field is significantly enhanced at plasmonic resonances.[14,24] These findings are fully consistent with the results already reported in Ref. 13.

The 2D rectangular patterns were then fabricated using a Raith150 e-beam lithography system operating at 20 kV. First a layer of primer was spin-coated at high speed (6000 rpm) in order to get a single monolayer to improve the adhesion of the following resist layers and avoid graphene interaction with contaminants. Then a bi-layer composed of a 500 nm-thick Polymethyl methacrylate (PMMA)-MA and 250 nm-thick PMMA layers was spin-coated on the sample and adopted as positive resist. The resulting 750 nm-thick resist layer ensures the presence of a good mask for the evaporation of the gold layer (150 nm) by means of a thermal evaporator with a current of 350 A and a deposition rate of about 1-2 Å/s. An adhesion layer of a few nanometers of chrome had been previously evaporated to improve the adhesion of the gold-on-graphene layers to the glass substrate. The sample was then immersed in an acetone bath for the lift-off process to release the final device. Figs. 3(a) and 3(b) show the Scanning Electron Microscope (SEM) images of the final device. In particular, the lower portion of Fig. 3(a) shows the 2D pattern still covered by the bi-layer and the evaporated metal layers. In the inset of the figure the final result of the lift-off process is clearly visualized. Moreover, the picture depicts a detail of the 2D pattern of rectangular patches where the graphene grain boundaries may be seen. This is due to the polycrystalline nature of the commercial substrate, which presents different crystallographic orientations. Fig. 3(b) shows the array having two periodicities $p_x = 630$ nm and $p_y = 780$ nm. The inset in Fig. 3(b) also shows that the commercial substrate contains small areas with material defects where multilayer graphene or graphite-like flakes are present (red circle).

An interesting aspect of the fabrication process was the relative simplicity of the e-beam writing process and the SEM inspection allowed by the graphene layer. Thanks to its high conductivity, graphene prevents the charging effect due the electron beam that is always present and evident in the insulator substrates (as in the glass in our case). This is very advantageous and leads to significant reduction of the number of technological steps required by avoiding thermal or electronic evaporation of thin metal layers (e.g., gold or chrome) before e-beam writing and SEM inspection.

The device was characterized by means of a Horiba Jobin-Yvon LabRAM HR-VIS micro-Raman spectrometer equipped with a 532 nm laser source. Fig. 4 shows the Raman spectra of the commercial CVD monolayer graphene transferred on glass substrate, acquired before any treatment (black curve) and after fabrication procedures on both bare and gold nanopatch-covered areas (red and blue lines, respectively). We point out that at approximately 1350 cm^{-1}, the pristine graphene spectrum does not exhibit the D peak, attesting for its high structural quality. Interestingly, after the fabrication process, this mode still shows a negligible contribution, indicating that the monolayer graphene has not been damaged.

Conversely, the consistent G peak red shift (from 1588 cm^{-1} to 1578 cm^{-1}) upon the Au fabricated array attests to a change in graphene transport properties. Specifically, the softening of Raman G mode may be related to a decrease in graphene carrier concentration (both for electron- or hole-doping).[25] Hole-doping has been typically demonstrated for pristine CVD-graphene samples owing to adsorption of air contaminants such as H_2O or CO_2 acting as electron-withdrawing.[26] Vacuum and thermal treatments involved in the Au array fabrication (electron beam lithography and thermal evaporation) could cause desorption. Thus, the observed red shift of the G mode may be related to the

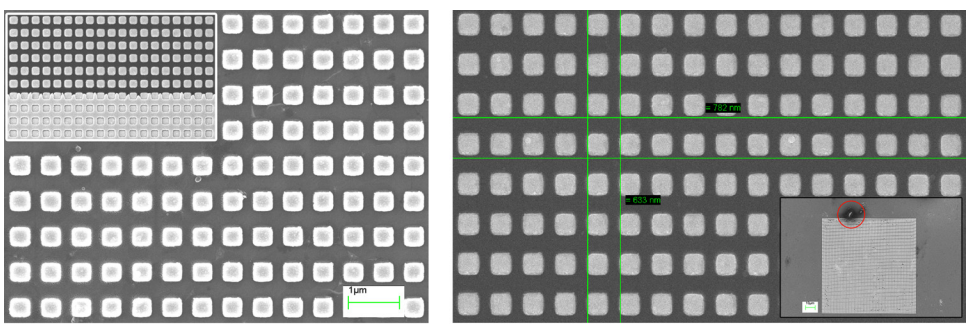

FIG. 3. Device fabrication: (a) detail with graphene grain boundaries (inset: lift-off process result); (b) final device with p_x and p_y equal to 630 nm and 780 nm, respectively; (inset) 2D array of rectangular nanopatches with a footprint of 100 μm x 100 μm. The red circle indicates the presence of a multilayer graphene or graphite-like areas in the transferred CVD monolayer graphene.

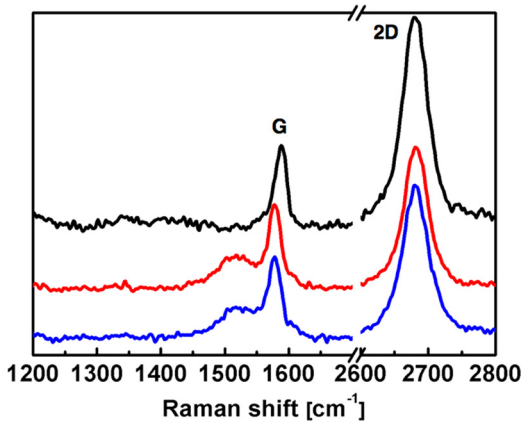

FIG. 4. Raman spectra of the commercial CVD graphene transferred on glass substrate acquired before any treatment (black curve) and after fabrication on both bare (red curve) and gold nanopatches-covered areas (blue curve). The curves have been shifted for a better view.

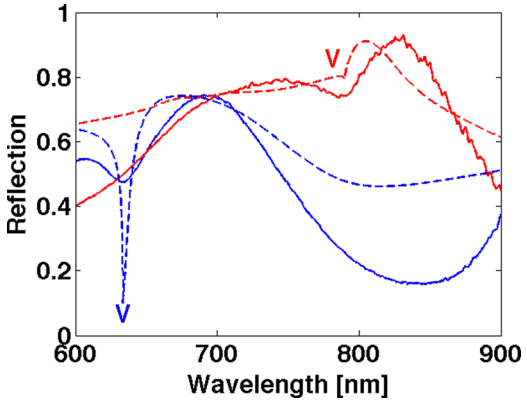

FIG. 5. Measured (solid curves) and simulated (dashed curves) reflection spectra for 0° ($p_x = 630$ nm, $a_x = 70$ nm, blue curves) and 90° ($p_y = 780$ nm, $a_y = 160$ nm, red curves), respectively.

suppression of the graphene intrinsic hole-doping. Indeed, vacuum annealing of graphene samples can help to remove adsorbates such as H_2O, NO_x, CO_2 and reduce its hole carrier density, as reported in literature.[26] However, when exposing the sample back to air, approximately the same doping level should be recovered. Interestingly, in our case, we did not observe any recovery of the D mode position after 2 weeks of air exposure. We assume that air contaminant/graphene interaction may be inhibited by surface chemical impurities deriving by the electron beam lithography and lift-off processes. Their presence is highlighted by the broad peak near 1520 cm^{-1}. Specifically, before any array fabrication step, graphene was treated by a resist primer consisting of a combination of PM acetate (80%) and hexamethyldisilazane (HDMS) (20%). This last step may strongly prevent the adsorption of dipolar substances on the graphene surface due to its hydrophobic character. This is supported by other experimental works that state that deposition of graphene on SiO_2 substrates treated by HMDS can provide graphene with low intrinsic doping levels even in ambient air.[25,26] Finally, the comparison between processed sample Raman spectra on bare and Au nanopatch-covered areas did not show any appreciable difference in G-peak position. This attests that the graphene's Fermi level is not locally influenced by the presence of the metal array. The absence of any doping effect is related to the presence of the chrome adhesion layer sandwiched between the gold and the graphene layers. The low mismatch between Cr (4.6 eV) and graphene (4.5 eV) work functions minimizes charge transfer processes.

The 2D array was finally characterized in the linear regime by means of the optical setup described in Ref. 27. A white-light lamp filtered in the 500 nm–900 nm range was focused on the sample by means of a low numerical-aperture, infinity-corrected microscope objective (10× and *Numerical Aperture*, $NA = 0.25$). The reflected light was collected by an aspherical fiber lens collimator and filtered by a linear polarizer. Finally, the filtered light was sent to an optical spectrometer (HR4000 from Ocean Optics) through a multimode optical fiber. The spectra normalization was carried out by using a flat gold surface as spectrum reference.

As expected from our simulations (see Fig. 2), the measured spectra are characterized by two different peaks (state *V* – Wood's anomaly) when the polarization angle is equal to 0° (polarization along p_x) and 90°(polarization along p_y). These dips are located at ∼633 nm and ∼788 nm, respectively (Fig. 5). For comparison, the simulation results are superimposed on the same plot when the gold nanopatch apertures a_x and a_y are equal to about 70 nm and 160 nm along the *x*-axis and *y*-axis direction, respectively.

As also reported in Refs. 27 and 28, plasmonic resonances are broadened with respect to numerical results because they are sensitive to light incident at an angle due to the microscope objective numerical aperture and to the gold surface roughness.

In conclusion, we have presented a complete theoretical and experimental study of gold rectangular nanopatches arranged in a two-dimensional periodic array grown on a graphene monolayer. We have shown that this system, based on a simple geometrical structure (nanopatches), offers the advantage of double plasmonic resonances related to the Wood anomaly. These resonances may be tuned by changing the periodicity and can be addressed by changing the polarization. Additionally, we have shown that these resonances act in a different way with respect to the structures reported in literature in Refs. 18 and 19. We have verified that these plasmonic resonances may be forced to interact with a single layer of absorbing material such as graphene. This interface strongly alters the optical properties in terms of absorption and resonance spectral position. These findings are consistent with the results already reported in literature[13] and reveal that it is possible to slightly tune the resonances by ∼1 nm and ∼10 nm for states *V* and *H*, respectively, in the particular case of the rectangular nanopatches. On the experimental side, the introduction of primer and adhesion layers prevents graphene contamination and doping, advantages that may be exploited in situations where the electrical and optical properties of the graphene must be preserved.

M. Grande thanks the U.S. Army International Technology Center Atlantic for financial support (W911NF-12-1-0292). This research was performed while the authors M. A. Vincenti and D. de Ceglia held a National Research Council Research Associateship

awards at the U.S. Army Aviation and Missile Research Development and Engineering Center.

[1]K. S. Novoselov, A. K. Geim, S. V. Morozov, D. Jiang, Y. Zhang, S. V. Dubonos, I. V. Grigorieva, and A. A. Firsov, Science **306**(5696), 666–669 (2004).
[2]V. G. Kravets, F. Schedin, R. Jalil, L. Britnell, R. V. Gorbachev, D. Ansell, B. Thackray, K. S. Novoselov, A. K. Geim, A. V. Kabashin, and A. N. Grigorenko, Nat. Mater. **12**, 304–309 (2013).
[3]A. N. Grigorenko, M. Polini, and K. S. Novoselov, Nat. Photonics **6**, 749–758 (2012).
[4]F. H. L. Koppens, D. E. Chang, and F. J. G. de Abajo, Nano Lett. **11**, 3370–3377 (2011).
[5]L. Ju, B. Geng, J. Horng, C. Girit, M. Martin, Z. Hao, H. A. Bechtel, X. Liang, A. Zettl, Y. R. Shen, and F. Wang, Nat. Nanotechnol. **6**, 630–634 (2011).
[6]A. Yu. Nikitin, F. Guinea, and L. Martin-Moreno, Appl. Phys. Lett. **101**, 151119 (2012).
[7]A. E. Nikolaenko, N. Papasimakis, E. Atmatzakis, Z. Luo, Z. Xiang Shen, F. De Angelis, S. A. Boden, E. Di Fabrizio, and N. I. Zheludev, Appl. Phys. Lett. **100**, 181109 (2012).
[8]X. Ling, L. Xie, Y. Fang, H. Xu, H. Zhang, J. Kong, M. S. Dresselhaus, J. Zhang, and Z. Liu, Nano Lett. **10**(2), 553–561 (2010).
[9]C. F. Schedin, E. Lidorikis, A. Lombardo, V. G. Kravets, A. K. Geim, A. N. Grigorenko, K. S. Novoselov, and A. C. Ferrari, ACS Nano **4**(10), 5617 (2010).
[10]T. Mueller, F. Xia, and P. Avouris, Nat. Photonics **4**, 297–301 (2010).
[11]B. Sensale-Rodriguez, R. Yan, M. Zhu, D. Jena, L. Liu, and H. G. Xin, Appl. Phys. Lett. **101**, 261115 (2012).
[12]D. T. J. Echtermeyer, L. Britnell, P. K. Jasons, A. Lombardo, R. V. Gorbachev, A. N. Grigorenko, A. K. Geim, A. C. Ferrari, and K. S. Novoselov, Nat. Commun. **2**, 458 (2011).
[13]B. V. G. Kravets, F. Schedin, R. Jalil, L. Britnell, K. S. Novoselov, and A. N. Grigorenko, J. Phys. Chem. C **116**(6), 3882 (2012).
[14]D. de Ceglia, M. A. Vincenti, M. Scalora, N. Akozbek, and M. J. Bloemer, AIP Adv. **1**, 032151 (2011).
[15]A. V. G. Kravets, F. Schedin, and A. N. Grigorenko, Phys. Rev. Lett. **101**, 087403 (2008).
[16]R. Marani, M. Grande, V. Marrocco, A. D'Orazio, V. Petruzzelli, M. A. Vincenti, and D. de Ceglia, Opt. Lett. **36**, 903–905 (2011).
[17]M. A. Vincenti, D. de Ceglia, M. Scalora, R. Marani, V. Marrocco, M. Grande, G. Morea, and A. D'Orazio, Proc. SPIE **7946**, 794625 (2011).
[18]Y. Chu, M. G. Banaee, and K. B. Crozier, ACS Nano **4**(5), 2804–2810 (2010).
[19]M. G. Banaee and K. B. Crozier, ACS Nano **5**(1), 307–314 (2011).
[20]COMSOL Multiphysics software.
[21]E. V. G. Kravets, A. N. Grigorenko, R. R. Nair, P. Blake, S. Anisimova, K. S. Novoselov, and A. K. Geim, Phys. Rev. B **81**, 155413 (2010).
[22]M. Bruna and S. Borini, Appl. Phys. Lett. **94**, 031901 (2009).
[23]E. D. Palik, *Handbook of Optical Constants of Solids* (Academic Press, San Diego, CA, 1998).
[24]M. Grande, R. Marani, F. Portincasa, G. Morea, V. Petruzzelli, A. D'Orazio, V. Marrocco, D. de Ceglia, and M. A. Vincenti, Sens. Actuators, B **160**(1), 1056–1062 (2011).
[25]A. Das, S. Pisana, B. Chakraborty, S. Piscanec, S. K. Saha, U. V. Waghmare, K. S. Novoselov, H. R. Krishnamurthy, A. K. Geim, A. C. Ferrari, and A. K. Sood, Nat. Nanotechnol. **3**, 210–215 (2008).
[26]M. Lafkioti, B. Krauss, T. Lohmann, U. Zschieschang, H. Klauk, K. v. Klitzing, and J. H. Smet, Nano Lett. **10**(4), 1149–1153 (2010).
[27]M. Grande, M. A. Vincenti, T. Stomeo, G. Morea, R. Marani, V. Marrocco, V. Petruzzelli, A. D'Orazio, R. Cingolani, M. De Vittorio, D. de Ceglia, and M. Scalora, Opt. Express **19**, 21385–21395 (2011).
[28]M. Grande, G. V. Bianco, M. A. Vincenti, T. Stomeo, D. de Ceglia, M. De Vittorio, V. Petruzzelli, M. Scalora, G. Bruno, and A. D'Orazio, Appl. Phys. Lett. **101**, 111606 (2012).